Effects of Soil Moisture on Temperatures, Winds, and Pollutant Concentrations in Los Angeles

MARK Z. JACOBSON

Department of Civil and Environmental Engineering, Stanford University, Stanford, California

(Manuscript received 17 October 1997, in final form 14 April 1998)

ABSTRACT

This paper examines the effects of soil moisture initialization in a coupled air quality–meteorological model on temperature profiles, wind speeds, and pollutant concentrations. Three simulations, each with different initial soil moisture fields, were run. In the baseline simulation, predicted temperatures, wind speeds, and gas/aerosol pollutant concentrations accurately matched observations. In the other two simulations, soil moisture contents were initialized about 4% lower and higher, respectively, than in the baseline simulation. In the low-moisture case, predicted temperature profiles were hotter, near-surface wind speeds were faster, and near-surface pollutant concentrations were lower than observations and baseline predictions. In the high-moisture case, predicted temperatures were colder, wind speeds were slower, and pollutant concentrations were higher than observations and baseline predictions. Initial soil moisture contents affected vertical temperature profiles up to 600-mb altitude after two days. Elevated temperature changes were due in part to changes in sensible heat fluxes from the surface and in part to changes in elevated heat advection fluxes. Changes in temperature profiles affected wind speeds and boundary layer depths, which affected times and magnitudes, respectively, of peak concentrations. Slower wind speeds, associated with high soil moisture contents, delayed times of peak concentrations in the eastern Los Angeles basin. Faster wind speeds, associated with low soil moisture contents, advanced times of peak concentrations. High soil moisture contents resulted in thinner boundary layer depths, increasing average near-surface pollutant concentrations, including that of ozone. Low soil moisture contents resulted in thicker boundary layer depths, decreasing average concentrations, including that of ozone. At some locations, changes in the magnitude of peak ozone concentrations depended on how changes in soil moisture affected ozone precursors and destroyers.

1. Introduction

Meteorological models predict changes in surface and deep soil moisture but require initial soil moisture fields as inputs. In most meteorological models, initial soil moisture fields are usually set to one value, a grid of best guesses, or a grid of estimates derived from a climatological database. In one such database (Mintz and Serafini 1992), global soil moisture fields were derived from observations of precipitation, radiation, temperature, specific humidity, and wind speed.

Ideal sources of soil moisture data for model initialization are measurements from remote sensing instruments. One instrument, the long wavelength microwave radiometer, measures emissivities from which soil moisture is extracted (Schmugge et al. 1974). This instrument has been used from an aircraft to map surface soil moisture fields over a local region (Schmugge 1996). Soil moisture has also been measured by a scanning multichannel microwave radiometer (SMMR) loaded onto the *Nimbus-7* satellite. The SMMR can resolve soil moisture with a spatial resolution of 150 km at 6.6 GHz down to 30 km at 37 GHz. Another instrument, the synthetic aperture radar, measures the backscattering coefficient of soil at a given wavelength. The backscattering coefficient varies with a soil's dielectric constant, which varies with soil moisture content (Ji et al. 1996). Soil moistures have also been derived from evaporation rates extracted from satellite surface temperature, albedo, vegetation index data (Bastiaanssen et al. 1997; van den Hurk et al. 1997), and from brightness temperatures measured by a microwave sensor loaded onto a satellite (Lakshmi et al. 1997).

Although remote sensing methods for obtaining soil moisture data have been developed, such data are currently available only for limited times and areas. It is also unclear whether a soil moisture field generated today could be used as a surrogate for a field 10 years ago at the same location. Thus, the modeling of past and most present meteorological and pollution episodes still requires estimates of soil moisture fields.

It is well known that initial soil moisture fields affect

Corresponding author address: Dr. Mark Z. Jacobson, Department of Civil and Environmental Engineering, Stanford University, Terman Engineering Center, M-13 Stanford, CA, 94305-4020.
E-mail: jacobson@ce.stanford.edu

meteorological model predictions. Soil moisture affects ground temperatures, which affect vertical temperature profiles. Temperature profiles affect boundary layer depths, pressures, and velocities. The effects of soil moisture variations on planetary boundary layer depth and circulation patterns have been studied by Zhang and Anthes (1982), Mahfouf et al. (1987), and Lanicci et al. (1987), among others. Lanicci et al. (1987), for example, found that low soil moisture over the Mexican plateau permitted formation of a deep mixed layer through strong surface heating and vertical mixing. The sensitivity of soil moisture variations on global-scale meteorology has been studied by Walker and Rowntree (1977), Rind (1982), and Mintz (1984), among others.

The sensitivity of ozone to certain land surface parameters other than soil moisture has been studied. Kessler and Sailor (1991) used a mesoscale model to examine the effects of changes in albedo (through roof and road painting) and sensible heat fluxes (through tree planting) on temperatures, wind speeds, and mixing heights in the Los Angeles basin. Taha (1996, 1997) extended this work by studying the effects of tree planting on ozone through changes in emissions and effects of surface albedo on ozone through changes in meteorology. Stern (1994) studied the effects of temperatures on ozone mixing ratios. No study to date has examined how changes in initial soil moisture fields affect concentrations of chemically produced and emitted gases and aerosols. It is hypothesized that changes in boundary layer depths and wind speeds resulting from small changes in soil moisture have relatively large effects on species concentrations. To test this hypothesis, simulations with a coupled air quality–meteorological model were carried out. The model is described and results are discussed herein.

2. Description of the model

The model used for this study was GATORM, a gas, aerosol, transport, radiation, and meteorological model [Jacobson 1994, 1997a,b, 1998, 1999; Jacobson et al. 1996]. The meteorological component was developed by Lu (1994; Lu and Turco 1995). GATORM is the first and only three-dimensional model in which gas, size-resolved aerosol, radiative, and meteorological predictions have been compared simultaneously with data from a comprehensive database (Jacobson 1994, 1997b) and the first gas/size-resolved aerosol air quality model to feed radiative heating rates back to a meteorological module for temperature calculations. The model has been used to study the effects of aerosols on near-surface temperatures (Jacobson 1997b), on vertical photolysis coefficient profiles, on vertical temperature profiles, and on near-surface ozone (Jacobson 1998). It has also been used to study development of elevated pollution layers in Los Angeles (Lu and Turco 1995).

GATORM solves the continuity equations for air, trace gases, aerosol number concentration, and aerosol volume concentration. It solves the thermodynamic energy equation, the horizontal momentum equations, the equation for geopotential, and a spectral form of the radiative transfer equation. Gases are affected by emissions, chemistry, dry deposition, gas-to-particle conversion, and transport. Size-resolved aerosols in the model are affected by emissions, coagulation, gas-to-particle conversion, internal reversible reactions, internal irreversible reactions, sedimentation, dry deposition, and transport.

The time variation in surface soil moisture and temperature is predicted with a 10-layer soil module (Lu 1994). The module solves the heat conduction equation and liquid water transport equation below the ground surface. At the surface, the heat conduction equation is modified to include the effects of net solar plus infrared radiative heat fluxes, turbulent sensible heat fluxes, and evaporative heat fluxes. The water transport equation at the surface is modified to account for evaporation and precipitation. In GATORM, gases, aerosols, and clouds affect optical depths, which affect downward and upward irradiances. They in turn affect ground temperatures and evaporation rates, which affect soil moisture fields. Thus, a feedback exists between pollutants and soil moisture.

In the soil module, the base of the deepest layer is 0.5 m. The moisture content of the deepest layer is initialized and held constant during a simulation period. Initial moisture contents of other layers are scaled linearly with depth to that of the deepest layer so that the moisture content of the top layer is 85% of that of the deepest layer. This scaling factor was determined by running the model for several days and using the average ratio of top to deep soil moisture found at 0330 LT during this period. Moisture contents for layers aside from the deepest are predicted after initialization.

3. Description of simulations

Simulations were carried out over the Los Angeles basin from 27 to 28 August 1987. Figure 1 shows a map of the region and monitoring sites pertinent to this study. The model grid's southwest corner was located at 32.97°N latitude and 119.25°W longitude. The horizontal, spherical coordinate grid included 66 west–east grid cells by 42 south–north cells. Grid spacing was 0.05° west–east (about 4.6 km) and 0.045° south–north (about 5.0 km). In the vertical, 20 sigma-pressure coordinate layers between the topographical surface and 250 mb were used. Approximately eight layers resided below 850 mb (1.5 km) altitude. The model treated 111 gases, 16 aerosol size bins (0.014–74 μm in diameter), and 36 components per bin. The gas- and aqueous-phase chemical mechanisms used for this study are given in Jacobson (1999). Gas and aerosol emissions rates are described in Jacobson (1998). Average soil specific heats, densities, albedos, and roughnesses for each grid cell were determined by summing, over all land use

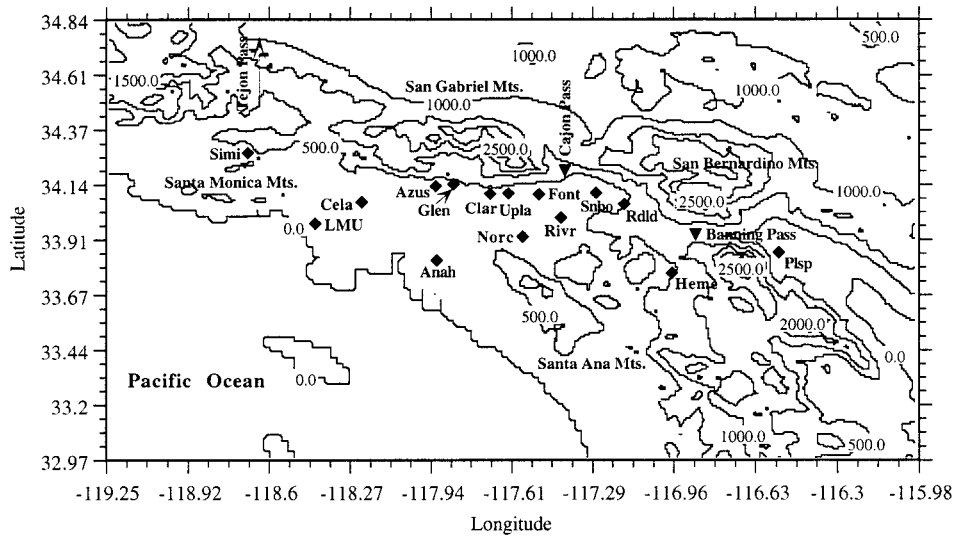

FIG. 1. Map of the Los Angeles basin modeling region used for this study. Monitoring site abbreviations are Simi (Simi Valley), Cela (Central Los Angeles), LMU (Loyola Marymount University), Azus (Azusa), Glen (Glendora), Anah (Anaheim), Clar (Claremont), Norc (Norco), Upla (Upland), Font (Fontana), Rivr (Riverside), Snbo (San Bernardino), Rdld (Redlands), Heme (Hemet), and Plsp (Palm Springs). Altitudes are in meters.

types in a grid cell, the product of the fractional land use and the estimated value of each parameter for the land use type. Such parameters were held constant in time and for all simulations but varied spatially.

Three simulations—a baseline, low soil moisture, and high soil moisture simulation—were run. In the baseline simulation, the initial deep soil moisture content was set to 23% (0.23 m^3, liquid H_2O; m^{-3}, soil) in land grid cells within 22 km of the coastline and 19% in all other land grid cells. The corresponding initial surface soil moisture contents were 85% of the deep moisture contents. In the low-moisture simulation, all land cells were initialized with deep soil moisture contents of 15%. In the high-moisture simulation, all land cells were initialized with deep soil moisture contents of 23%. Table 1 summarizes the initial deep and surface soil moisture contents for the three cases. Additional sensitivity tests, not shown, in which coastal moisture was set differently from inland moisture, supported the fundamental conclusions that follow.

Predictions from simulations were compared with data from the Southern California Air Quality Study (e.g., Lawson 1990). During the study, gas, aerosol, meteorological, and radiative parameters were measured. Details of the data used for comparison in this study are given in Jacobson (1997b).

TABLE 1. Initial surface and deep (0.5 m) soil moisture contents (%) within 22 km of the coastline and inland for the baseline case and two sensitivity cases.

	Baseline case		Low-moisture case		High-moisture case	
	Near coast	Inland	Near coast	Inland	Near coast	Inland
Surface moisture	19.6	16.2	12.8	12.8	19.6	19.6
Deep moisture	23	19	15	15	23	23

4. Results

Figures 2a–c show variations in predicted surface soil moisture contents at Loyola Marymount, Riverside, and Palm Springs, respectively, for each of the three simulations. Each location is successively farther inland than the last, as shown in Fig. 1. During the day and night, surface soil moisture varied cyclically due to water diffusion to and from deep layers of soil, evaporation and/or condensation. For a given simulation, surface soil moisture contents generally decreased from the coast to desert, even when initial soil moisture content was constant everywhere. This occurred because water evaporated more readily from desert soil than coastal soil due to higher temperatures and lower specific humidities over the desert. Figure 3 shows a surface contour map of the predicted surface soil moisture field from the baseline case at 1530 PST 27 August 1987, which demonstrates a general decrease in soil moisture from the coast to desert. Soil moisture values can range from less than 2% to their saturation value, which vary from 39.5% for sand to 48.2% for clay (e.g., Clapp and Hornberger 1978). While predicted soil moisture contents in Los Angeles always fell well within this large range, the lack of spatially distributed or time-dependent soil moisture data for Los Angeles prevented a comparison of predicted with observed values.

Table 2 shows statistical comparisons of predictions

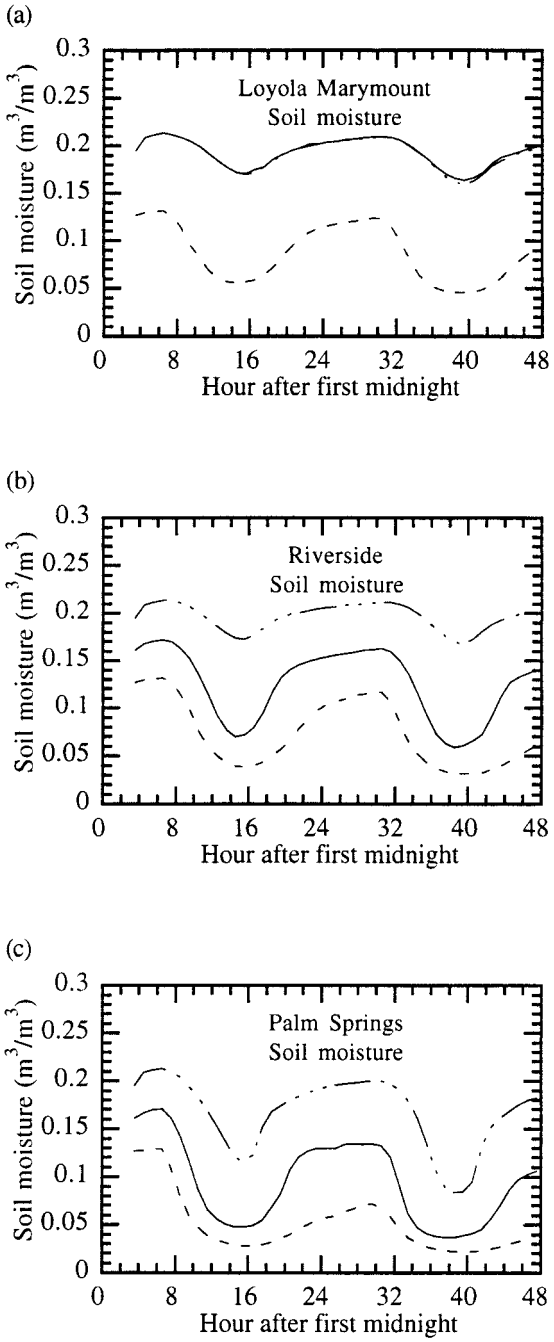

FIG. 2. Predicted surface soil moisture contents at three locations. The solid line (———) is the baseline case, the dashed line (– – –) is the initial 15% deep soil moisture simulation, and the dashed-dot line (– · · · –) is the initial 23% deep soil moisture case. The initial deep soil moisture field at Loyola Marymount was 23% in both the baseline and high soil moisture cases.

with observations for parameters other than soil moisture from the three simulations. The statistics include normalized gross error (absolute-value difference between a predicted and an observed value, divided by the observed value, summed over all comparisons, and divided by the number of comparisons) and normalized bias (same as normalized gross error, except no absolute value is taken). For most parameters, all observations were included in the statistical comparison. For some parameters (identified in the caption for Table 2), particularly certain gases and particle components, comparisons were made only when the observation exceeded a threshold or cutoff value (also identified in the caption). Below, statistics and time series plots are discussed in terms of the effects of soil moisture on near-surface temperatures, vertical temperature profiles, near-surface wind speeds, and pollutant concentrations, respectively.

a. Near-surface temperatures

Table 2 shows that near-surface air temperatures were overpredicted in the low-moisture case, underpredicted in the high-moisture case, and underpredicted to a lesser extent but most accurate in the baseline case. Soil consists of air, liquid water, and soil. The specific heat of liquid water is much larger than that of air or soil. Thus, the smaller the liquid water content of soil, the greater the increase in ground temperature during the day per unit of solar radiation absorbed, and the greater the decrease in ground temperature during the night per unit of infrared radiation emitted. Also, the smaller the liquid water content of soil, the smaller the rate of evaporation of water to the air (or greater the rate of condensation of water vapor to the ground), and the smaller the cooling (larger the warming) of the ground due to latent heat absorption (release). True to theory, near-surface air temperature predictions in the low-moisture simulation were higher than those in the baseline simulation and high-moisture simulation during the day. This fact is illustrated in Figs. 4a–c, which show temporal variations in predicted versus observed near-surface temperatures. During the night, soil moisture content had a much smaller effect on near-surface temperatures than during the day.

b. Vertical temperature profiles

Figures 5a–d show the effects of soil moisture on vertical temperature profiles. The baseline moisture content case resulted in the most accurate profile predictions. At Palm Springs, for example, the predicted baseline profile matched the observed profile almost exactly. In the low-moisture case, temperatures were generally overpredicted. In the high-moisture case, temperatures were generally underpredicted.

The figures indicate that soil moisture affected vertical temperature profiles by the second day up to 600 mb altitude. Above the boundary layer, many of the changes in temperature near the coast were due to changes in advective heat fluxes. This theory is supported in Fig. 5a. The figure shows that, in the high-moisture case at Loyola Marymount (LMU), elevated

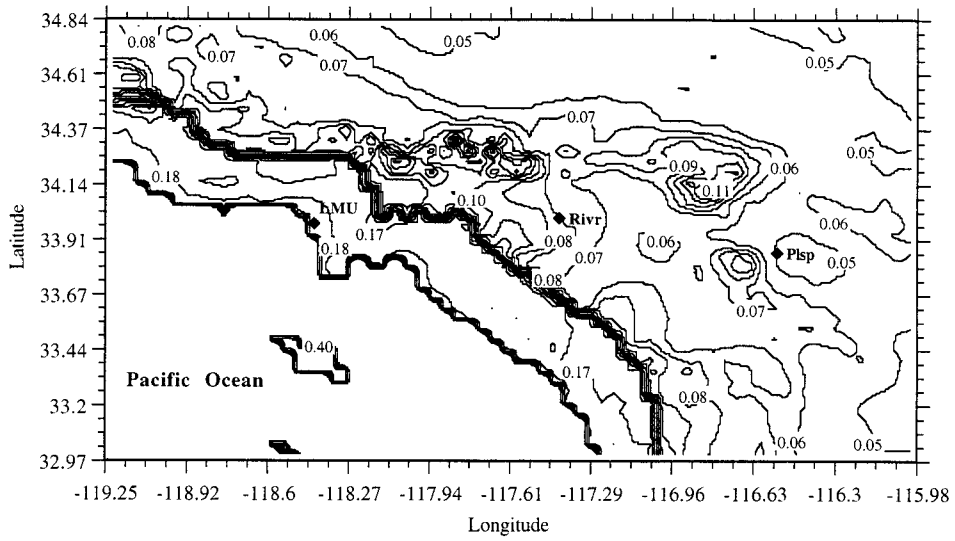

FIG. 3. Surface contour map of soil moisture content ($m^3\ m^{-3}$) at 1530 PST 27 Aug 1987 predicted from the baseline simulation. LMU (Loyola Marymount University), Rivr (Riverside), and Plsp (Palm Springs) are shown for reference.

TABLE 2. Normalized gross errors (NGEs) and normalized biases (NBs) for the baseline simulation and two sensitivity tests, averaged over the 44-h model simulation. The subscripts (10) and (2.5) indicate the mass of the species that resides in particles <10 μm or <2.5 μm in diameter, respectively. Mass is total particle mass, EC is elemental carbon, OC is organic carbon, solar rad is the sum of surface solar radiation (W m^{-2}) at <5-μm wavelength, σ_{sp} is the extinction coefficient due to scattering by particles, and σ_{ap} is the extinction coefficient due to absorption by particles. Cutoff mixing ratios were 50 ppbv for O_3 (g), 5 ppbv for SO_2 (g), 5 ppbv for HCHO (g), 1 ppbv for NH_3 (g), and 3 ppbv for HNO_3 (g). Additional cutoff values were 0.5 μg m^{-3} for sub-10-μm chloride, 0.3 μg m^{-3} for sub-2.5-μm ammonium, 10 W m^{-2} for solar radiation, and 0 for all other parameters.

		Baseline		15% deep soil moisture		23% deep soil moisture	
Parameter	Number of comparisons	NGE (%)	NB (%)	NGE (%)	NB (%)	NGE (%)	NB (%)
$Mass_{10}$	360	37.3	7.9	37.3	−0.1	64.3	49.7
$Mass_{2.5}$	356	35.1	−8.8	42.4	−9.5	68.3	49.9
EC_{10}	356	39.2	−29.0	45.5	−38.7	34.8	−10.8
$EC_{2.5}$	356	37.0	−20.0	40.7	−30.9	36.8	3.4
OC_{10}	352	33.5	3.6	36.2	−12.9	81.4	72.5
$OC_{2.5}$	352	32.9	−1.0	43.3	−17.9	96.6	88.2
Na_{10}	360	18.6	−8.5	17.8	−10.4	20.6	−10.7
$NH_{4_{10}}$	325	41.9	−24.3	51.6	−34.5	40.1	4.9
$NH_{4_{2.5}}$	321	56.4	−17.4	63.3	−22.6	60.7	16.6
$SO_{4_{10}}$	360	27.5	−10.7	33.8	−19.6	30.5	6.7
$SO_{4_{2.5}}$	360	30.5	0.6	35.0	−9.6	40.1	21.8
$NO_{3_{10}}$	360	44.4	4.4	53.9	−8.7	73.7	26.9
$NO_{3_{2.5}}$	360	56.6	−37.6	62.4	−41.7	79.4	−11.9
Cl_{10}	190	56.4	−56.1	49.6	−48.8	56.6	−52.4
O_3 (g)	665	31.5	−4.2	40.0	−20.1	33.1	5.0
SO_2 (g)	339	35.9	−11.2	62.4	−58.2	49.3	−43.6
NH_3 (g)	269	73.7	−58.2	88.0	−37.3	92.1	−66.0
HNO_3 (g)	109	50.8	−24.5	78.0	−58.2	99.5	84.7
HCHO (g)	61	38.4	10.3	60.5	−47.8	96.4	94.9
Temperature	718	0.59	−0.33	0.91	0.5	0.70	−0.40
Surface pressure	409	0.31	0.10	0.30	0.08	0.32	0.10
Relative humidity	429	23.6	20.4	26.0	−19.3	31.5	28.2
Wind speed	584	36.9	−1.3	44.5	23.3	36.6	−26.4
Solar radiation	127	12.3	6.2	12.9	9.3	13.7	6.3
σ_{sp}	125	40.7	−6.8	47.8	−22.9	48.5	8.3
σ_{ap}	352	38.2	14.4	33.1	−5.0	54.8	37.2

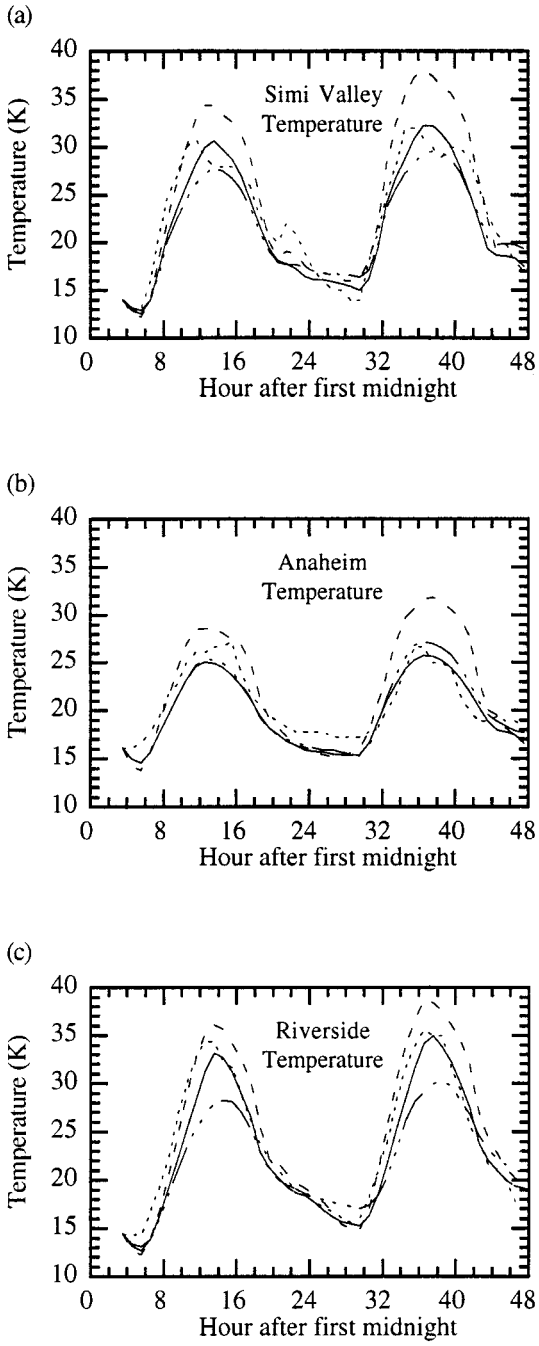

FIG. 4. Time series comparisons of predicted with observed near-surface temperatures. The solid line (———) is the baseline case, the dashed line (– – –) is the initial 15% deep soil moisture simulation, the dashed-dot line (– · · · –) is the initial 23% deep soil moisture case, and the dotted line [- - - (etc.)] is the observation.

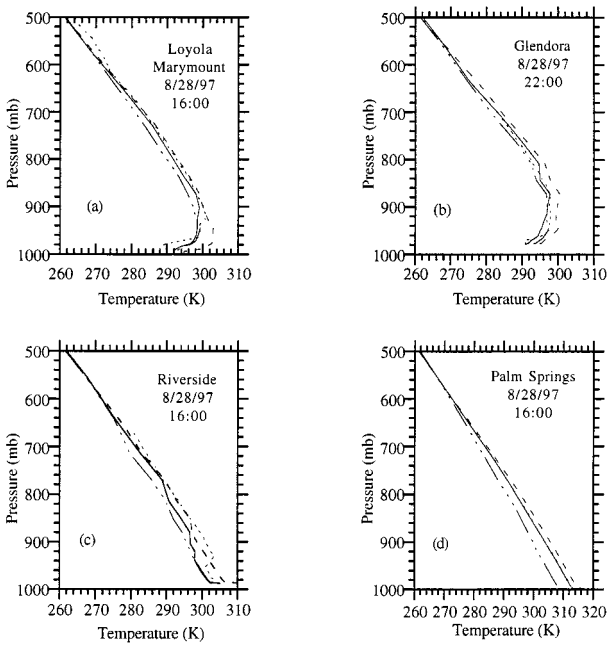

FIG. 5. Vertical profile comparisons of predicted with observed temperatures at four locations on 28 Aug. The simulations were initialized at 0330 PST 27 Aug. The solid line (———) is the baseline case, the dashed line (– – –) is the initial 15% deep soil moisture simulation, the dashed-dot line (– · · · –) is the initial 23% deep soil moisture case, and the dotted line [- - - (etc.)] is the observation. The baseline prediction and observation at Palm Springs lie on top of one another.

temperatures were lower than and boundary layer temperature were nearly the same as in the baseline case. Boundary layer temperatures were nearly the same since initial deep soil moisture in the baseline and high-moisture cases were both 23% at LMU (all locations within 22 km of the coastline were initialized with 23% deep soil moisture in the baseline simulation). Figure 2a shows that, over time, predicted surface soil moisture contents at LMU for the baseline and high-moisture cases remained similar to each other. Because soil moisture contents and boundary layer temperatures were invariant in both cases at LMU, the large differences in elevated temperatures must have been due to elevated heat advection. Cooler elevated temperatures above LMU in the high-moisture case resulted because high (relative to the baseline case) soil moisture contents in the desert, beyond the basin cooled elevated temperatures over the desert (e.g., Fig. 5d) through reductions in thermal turbulence. Strong, elevated flow advected this relatively cooler air from the desert to Loyola Marymount. In a similar manner, cool (relative to the baseline case) air aloft advected from the east to Palm Springs, enhancing the cooling at Palm Springs.

c. Near-surface wind speeds

Table 2 shows that the baseline simulation resulted in the most accurate predictions of daytime near-surface wind speeds. The low-moisture case resulted in the highest daytime wind speeds, and the high-moisture case resulted in the lowest daytime wind speeds. Figures 6a–g show these results in the form of time series plots. Decreases in soil moisture contents, such as between the

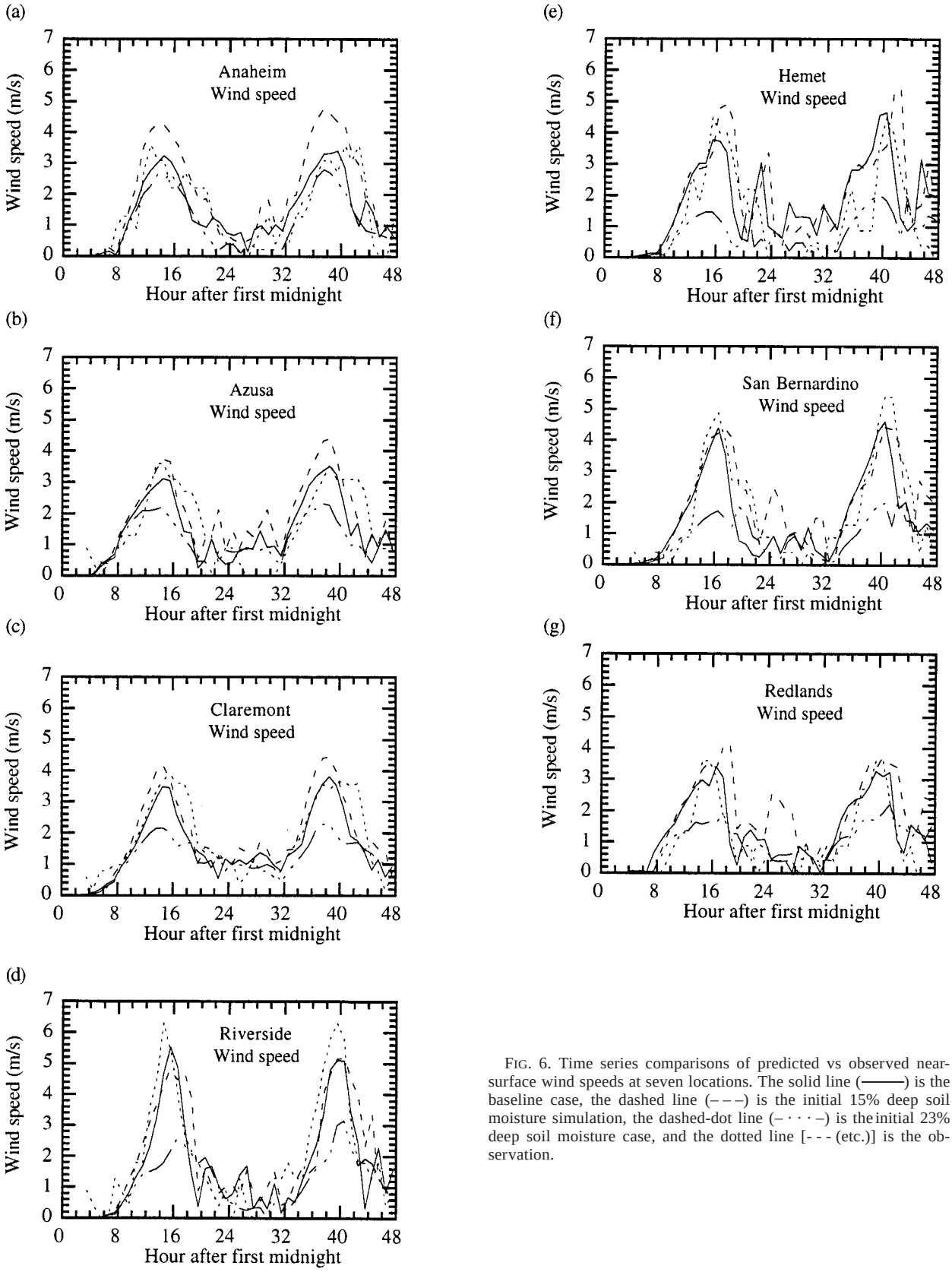

FIG. 6. Time series comparisons of predicted vs observed near-surface wind speeds at seven locations. The solid line (———) is the baseline case, the dashed line (– – –) is the initial 15% deep soil moisture simulation, the dashed-dot line (– · · · –) is the initial 23% deep soil moisture case, and the dotted line [- - - (etc.)] is the observation.

high- and low-moisture cases, increased daytime near-surface wind speeds by enhancing pressure gradients between the coast and desert. Decreases in soil moisture contents over the desert increased afternoon ground temperatures between the two cases by about 8 K. The corresponding increase near the coast was only about 3 K. The larger increase over the desert enhanced thermal turbulence and elevated horizontal divergence, decreasing air pressures over the desert relative to over the coast. Much of the diverging air returned toward the coast, where it increased air pressures. The resulting enhanced pressure gradient between the coast and desert increased near-surface wind speeds between the two cases.

A second mechanism by which wind speeds increased in the low-moisture case was by enhanced vertical mixing of horizontal momentum. Wind speeds are generally faster aloft than near the surface. Low soil moisture contents increased ground temperatures and thermal turbulence, increasing turbulent transport of momentum from aloft to the surface.

d. Pollutant concentrations

Table 2 shows that the low-moisture case resulted in strong underpredictions in gas and aerosol concentrations, the high-moisture case resulted in weaker underpredictions or overpredictions of such concentrations, and the baseline simulation resulted in intermediate results. When the moisture content was relatively low, ground temperatures were warmer, the atmosphere was more buoyantly unstable, pollutants mixed to a greater height, and near-surface concentrations were lower than when the moisture content was relatively high. When the moisture content was high, ground temperatures were cooler, vertical mixing was suppressed, and near-surface concentrations built up. Table 2 supports these theories with respect to average gas and aerosol concentrations (or mixing ratios).

Average ozone concentrations also increased with high soil moisture content and decreased with low soil moisture content. At a few locations and times, peak ozone concentrations did not follow the trend of the average. Figures 7a–f show time comparisons of predicted ozone mixing ratios from the baseline and sensitivity simulations with observations. At Fontana, Upland, and San Bernardino, peak ozone mixing ratios on the second day in the low soil moisture case were greater than those in the high-moisture and baseline cases, contrary to what was expected. The exact cause of the reversal is unclear, but it is believed that the low soil moisture contents resulted in a redistribution of ozone precursors and destroyers through faster wind speeds, increases in temperature, and thicker boundary layer depths. Faster wind speeds rapidly transported ozone precursors and destroyers to the eastern basin. Temperature changes affected reaction rate coefficients, resulting in ozone mixing ratio changes. Thicker boundary layer depths decreased mixing ratios of NO, resulting in less destruction of O_3 through the reaction $NO + O_3 \rightarrow NO_2 + O_2$. At the same time, reduced NO resulted in reduced chemical NO_2 production and reduced O_3 production through NO_2 photolysis. Cases of high ozone in the low-moisture simulation indicate that the dilution of NO had a greater effect on O_3 than reduced O_3 production.

Soil moisture affected times of peak pollutant mixing ratios. Slow wind speeds (as shown in Figs. 6a–g), resulting from high soil moisture contents, delayed ozone mixing ratio peaks in the eastern Los Angeles basin in comparison with the baseline simulation. In the high-moisture case, peaks generally, but not always, occurred before those in the baseline case. When the peak mixing ratio of ozone was delayed, the magnitude of ozone may have been affected by differences in gas emission rates between the original and delayed time of the peak. For instance, the ozone mixing ratio peak at Riverside was delayed by one hour on the second day of the low-moisture case in comparison with the baseline case (Fig. 7d). During that hour, emission rates of NO decreased at Riverside, possibly contributing to the higher O_3 mixing ratio in the delayed peak (since NO titrates O_3). Since factors aside from NO reaction with O_3 affect peak O_3 concentrations, as discussed previously, the emissions effect may be only part of the explanation for the increased value of the delayed O_3 peak at Riverside.

5. Conclusions

This paper examined the effects of soil moisture initialization in an Eulerian air pollution model on ozone, temperature, and wind speed predictions. Three simulations, each with different initial soil moisture fields, were run. In the baseline simulation, predicted ozone, temperature, wind speeds, and other parameters matched observations most accurately. In the other two simulations, soil moisture contents were initialized about 4% lower and higher, respectively, than in the baseline simulation. In the low-moisture case, predicted ozone was higher, temperatures were hotter, and wind speeds were faster than observations and baseline predictions. In the high soil moisture case, predicted ozone was higher, temperatures were colder, and wind speeds were slower than observations and baseline predictions. Initial soil moisture contents affected vertical temperature profiles up to 600 mb altitude. The elevated changes were due to changes in vertical sensible heat fluxes and elevated advection fluxes. Changes in temperature profiles affected boundary layer depths and wind speeds, which affected gas and aerosol concentrations and the time of peak concentrations, respectively. While the general findings of this study may apply to simulations at different times and locations, specific findings are likely to differ, since soil moisture is affected by radiative fields, evaporative fluxes, and ground temperatures, which vary with time and location.

Acknowledgments. A portion of this work was per-

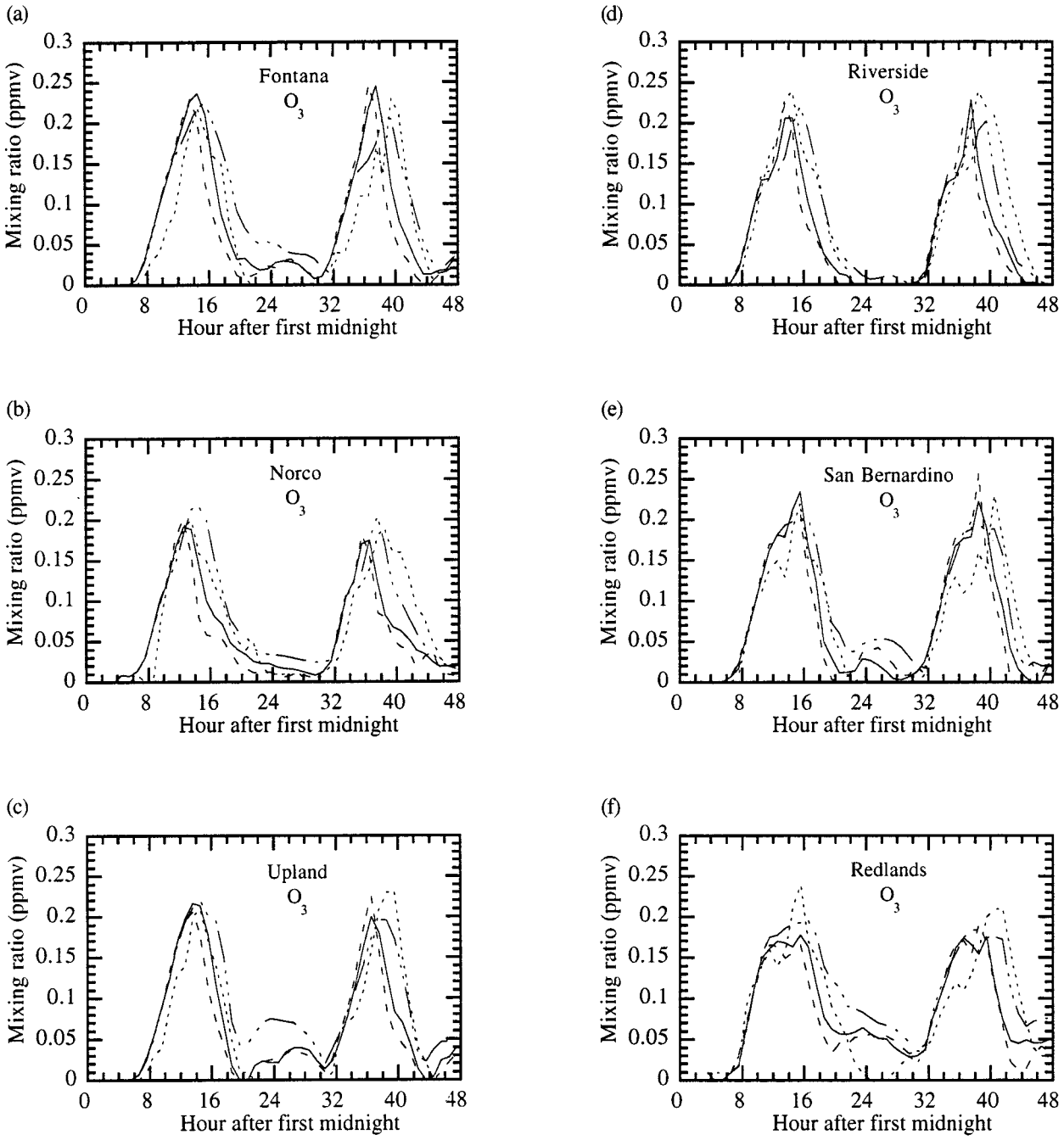

FIG. 7. Time series comparisons of predicted with observed near-surface ozone mixing ratios at six locations. The solid line (———) is the baseline case, the dashed line (– – –) is the initial 15% deep soil moisture simulation, the dashed-dot line (– · · · –) is the initial 23% deep soil moisture case, and the dotted line [- - - (etc.)] is the observation.

formed on a Cray J-916, provided in part by Cray Research, Inc. Cray 90 computer support was also given by the NAS computer facilities in Mountain View, California. This work was supported, in part, by grants from the Environmental Protection Agency under assistance Agreement 823186-01-0 and the National Science Foundation under Agreements ATM-9504481 and ATM-9614118.

REFERENCES

Bastiaanssen, W. G. M., H. Pelgrum, P. Droogers, H. A. R. de Bruin, and M. Menenti, 1997: Area-average estimates of evaporation, wetness indicators and top soil moisture during two golden days in EFEDA. *Agric. For. Meteor.*, **87,** 119–137.

Clapp, R. B., and G. M. Hornberger, 1978: Empirical equations for some soil hydraulic properties. *Water Resour. Res.*, **14,** 601–604.

Jacobson, M. Z., 1994: Developing, coupling, and applying a gas, aerosol, transport, and radiation model to study urban and regional air pollution. Ph.D. thesis, University of California, Los Angeles, 436 pp. [Available from UMI Dissertation Information Service, 300 North Zeeb Road, P.O. Box 1346, Ann Arbor, MI 48106-1346.]

——, 1997a: Development and application of a new air pollution modeling system—Part II. Aerosol module structure and design. *Atmos. Environ.,* **31,** 131–144.

——, 1997b: Development and application of a new air pollution modeling system—Part III. Aerosol-phase simulations. *Atmos. Environ.,* **31,** 587–608.

——, 1998: Studying the effects of aerosols on vertical photolysis rate coefficient and temperature profiles over an urban airshed. *J. Geophys. Res.,* **103,** 10 593–10 604.

——, 1999: *Fundamentals of Atmospheric Modeling.* Cambridge University Press, 656 pp.

——, R. Lu, R. P. Turco, and O. B. Toon, 1996: Development and application of a new air pollution modeling system—Part I. Gas-phase simulations. *Atmos. Environ.,* **30B,** 1939–1963.

Ji, J., P. van der Keur, A. Thomsen, and H. Skriver, 1996: Soil moisture retrieval using the Danish L- and C-band polarimetric SAR. *Proc. 1996 Int. Geoscience and Remote Sensing Symp.,* Lincoln, NE, 1300–1302.

Kessler, R. C., and D. J. Sailor, 1991: Use of numerical models to assess the effects of energy usage reduction measures on air quality in the Los Angeles basin. *Proc. 1991 U.S. EPA/AWMA Int. Symp. on the Role of Meteorology in Managing the Environment in the 90s,* Pittsburgh, PA, AWMA, 200–209.

Lakshmi, V., E. F. Wood, and B. J. Choudhury, 1997: Evaluation of Special Sensor Microwave/Imager satellite data for regional soil moisture estimation over the Red River basin. *J. Appl. Meteor.,* **36,** 1309–1328.

Lanicci, J. M., T. N. Carlson, and T. T. Warner, 1987: Sensitivity of the Great Plains severe-storm environment to soil-moisture distribution. *Mon. Wea. Rev.,* **115,** 2660–2673.

Lawson, D. R., 1990: The Southern California air quality study. *J. Air Waste Manag. Assoc.,* **40,** 156–165.

Lu, R., 1994: Development of an integrated air pollution modeling system and simulations of ozone distributions over the Los Angeles basin. Ph.D. thesis, University of California, Los Angeles, 362 pp. [Available from UMI Dissertation Information Service, 300 North Zeeb Road, P.O. Box 1346, Ann Arbor, MI 48106-1346.]

——, and R. P. Turco, 1995: Air pollutant transport in a coastal environment, II: Three-dimensional simulations over Los Angeles basin. *Atmos. Environ.,* **29,** 1499–1518.

Mahfouf, J.-F., E. Richard, and P. Mascart, 1987: The influence of soil and vegetation on the development of mesoscale circulations. *J. Appl. Meteor.,* **26,** 1483–1495.

Mintz, Y., 1984: The sensitivity of numerically simulated climates to land surface conditions. *The Global Climate,* J. Houghton, Ed., Cambridge University Press, 79–105.

——, and Y. V. Serafini, 1992: A global climatology of soil moisture and water balance. *Climate Dyn.,* **8,** 13–27.

Rind, D., 1982: The influence of ground moisture conditions in North America on summer climate as modeled in the GISS GCM. *Mon. Wea. Rev.,* **110,** 1487–1494.

Schmugge, T., 1996: Applications of passive microwave observations of surface soil moisture. *Proc. 1996 Int. Geoscience and Remote Sensing Symp.,* Lincoln, NE, 1051–1053.

——, P. Gloersen, T. T. Wilheit, and F. Geiger, 1974: Remote sensing of soil moisture with microwave radiometers. *J. Geophys. Res.,* **79,** 317–323.

Stern, R., 1994: *Entwicklung und anwendung eines dreidimensionalen photochemischen ausbreitungsmodells mit verschiedenen chemischen mechanismem.* Meteorologische Abhandlungen Serie A Band 8, Heft 1, Verlag von Dietrich Reimer.

Taha, H., 1996: Modeling impacts of increased urban vegetation on ozone air quality in the South Coast Air Basin. *Atmos. Environ.,* **30,** 3423–3430.

——, 1997: Modeling the impacts of large-scale albedo changes on ozone air quality in the South Coast Air Basin. *Atmos. Environ.,* **31,** 1667–1676.

van den Hurk, B. J. J. M., W. G. M. Bastiaanssen, H. Pelgrum, and E. van Meijgaard, 1997: A new methodology for assimilation of initial soil moisture fields in weather prediction models using Meteosat and NOAA data. *J. Appl. Meteor.,* **36,** 1271–1283.

Walker, J., and P. R. Rowntree, 1977: The effect of soil moisture on circulation and rainfall in a tropical model. *Quart. J. Roy. Meteor. Soc.,* **103,** 29–46.

Zhang, D., and R. A. Anthes, 1982: A high-resolution model of the planetary boundary layer—Sensitivity tests and comparisons with SESAME-79 data. *J. Appl. Meteor.,* **21,** 1594–1609.